

Figure S1. Transient exposure to ammonia inhibits activity in the preBötzing complex in the anesthetized rat.

A puff of ammonia suppresses rhythmic bursts in preBötzing cells, which constitute the core of the inspiratory central pattern generator for breathing. The recording site in the preBötzing is labeled by a deposit of the dye Chicago sky blue.

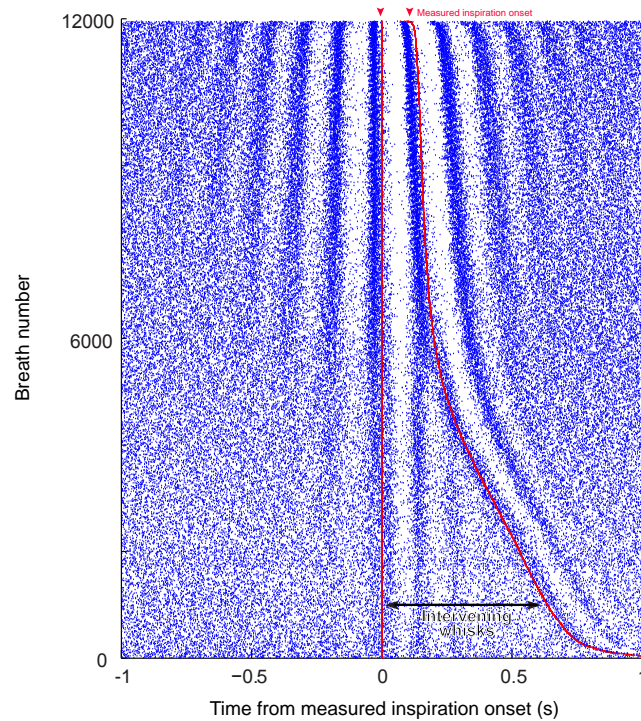


Figure S2. Coordination of whisking and breathing in one rat.

Temporal relationship between whisking and breathing events. Raster plots of inspiration and protraction onset times relative to each breath are sorted by the duration of the breath. In an individual animal, the intrinsic whisking oscillation frequency is stable and locked to the measured breathing onset time at both basal respiratory frequencies as well as sniffing frequencies. During basal respiration, the first, second, and third whisks following inspiratory drive occur at stereotypic times relative to breathing.

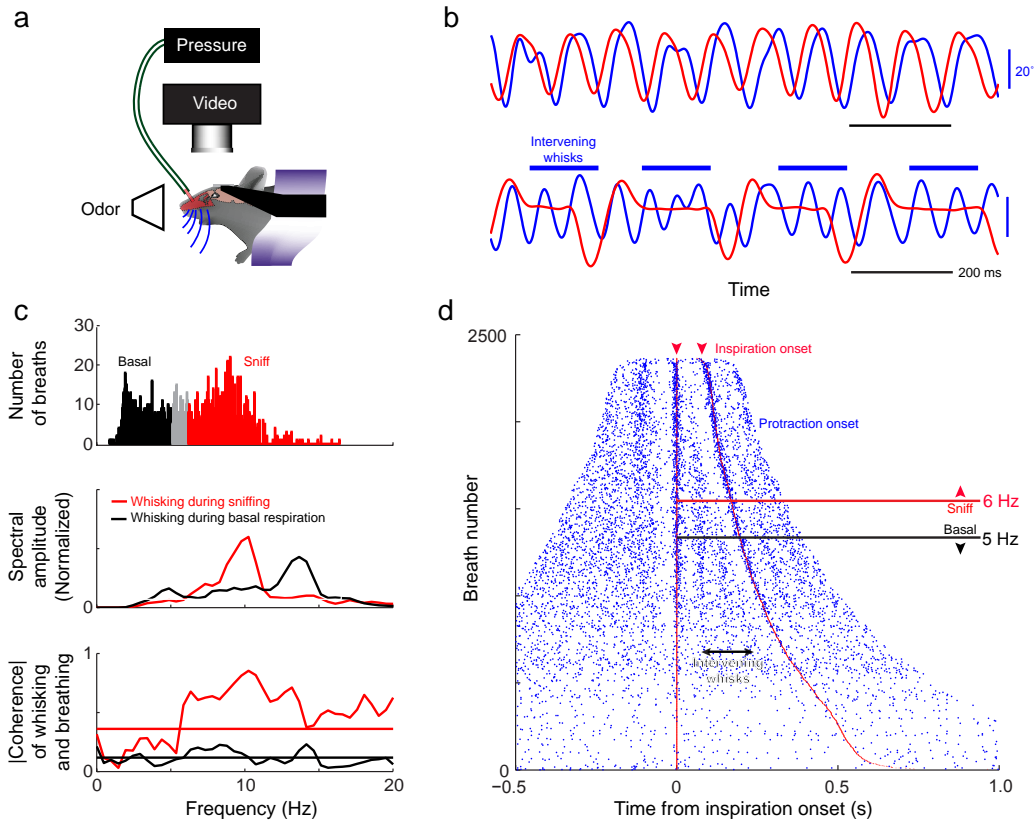


Figure S3. Coordination of whisking and breathing in mice.

(a) Experimental procedures to measure whisking and breathing. Head-restrained mice were implanted with a pressure transducer in the nasal cavity¹, and vibrissae were monitored with high speed videography.

(b) Simultaneous measurement of whisking and breathing. Vibrissa C2 position is in blue and pressure is in red. Protraction and inspiration are upward. During sniffing, inspiration is synchronous with vibrissa protraction on each cycle (top). During basal respiration, whisking is faster than breathing but inspiration remains synchronous with protraction (bottom).

(c) Spectral relationship between whisking and breathing. Histogram of instantaneous breathing frequency for each breath (top). Breathing rates above 6 Hz are classified as sniffing, and below 5 Hz are classified as basal respiration. Whisking spectra are plotted for periods of sniffing (red) and periods of basal respiration (black). Coherence between whisking and breathing for periods of sniffing and periods of basal respiration. Dashed lines represent thresholds for statistical significance ($p < 0.05$).

(d) Temporal relationship between whisking and breathing events. Raster plots of inspiration and protraction onset times relative to each breath are sorted by the duration of the breath, as in **Figure 1**. At high respiratory rates, whisking and breathing show a 1:1 relationship, but at lower frequencies there are intervening whisks between breaths. These data refute the claims of Cao, Roy, Sachdev and Heck (2012, Dynamic correlation between whisking and breathing rhythms in mice. *J Neurosci* 32, 1653-1659).

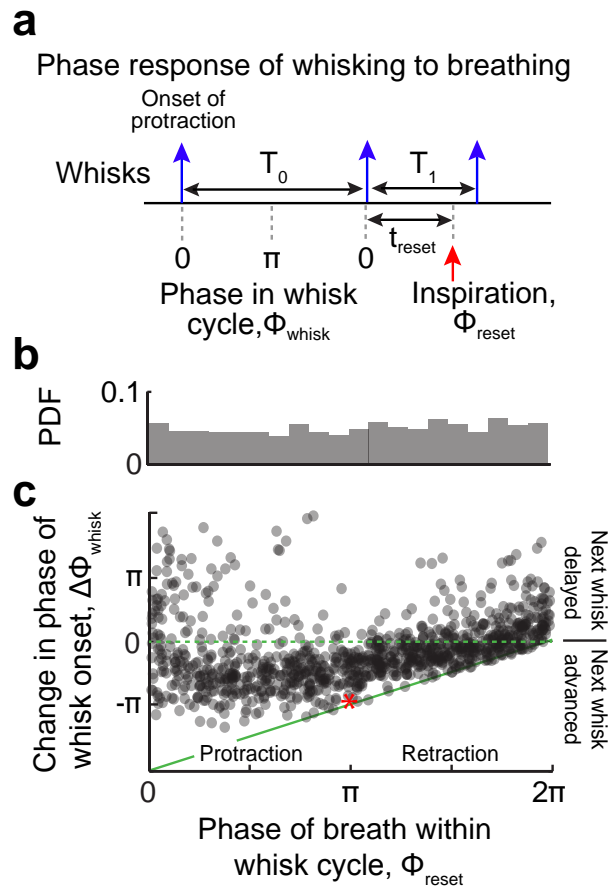


Figure S4. Phase resetting of whisking by breathing

(a) Schematic describing the phase-response of whisking relative to the onset of inspiration. For each whisk, the time at which inspiration occurs after the onset of protraction is defined as t_{reset} ; in this analysis inspiration plays the role of an external perturbation. The expected duration of the whisk is denoted by T_0 and, as the whisking frequency is stable throughout a bout, is taken as the duration of the preceding whisk. The duration of the perturbed whisk is denoted by T_1 . These times are normalized as the phase of the breath within the whisk cycle, defined by

$$\phi_{\text{reset}} = 2\pi(t_{\text{reset}} / T_0)$$

along with the resultant change in whisking phase, defined by

$$\Delta\phi_{\text{whisk}} = 2\pi(T_1 - T_0) / T_1.$$

(b) Probability density of ϕ_{reset} during basal respiration. Inspiration occurs at all phases of the whisking rhythm during basal respiration.

(c) Phase response of whisking to the onset of inspiratory drive during basal respiration. Onset times are adjusted as shown in **Figure 1d**. Symbols are defined above. The red asterisk represents the calculated perturbation for the example in the time-line in panel a.

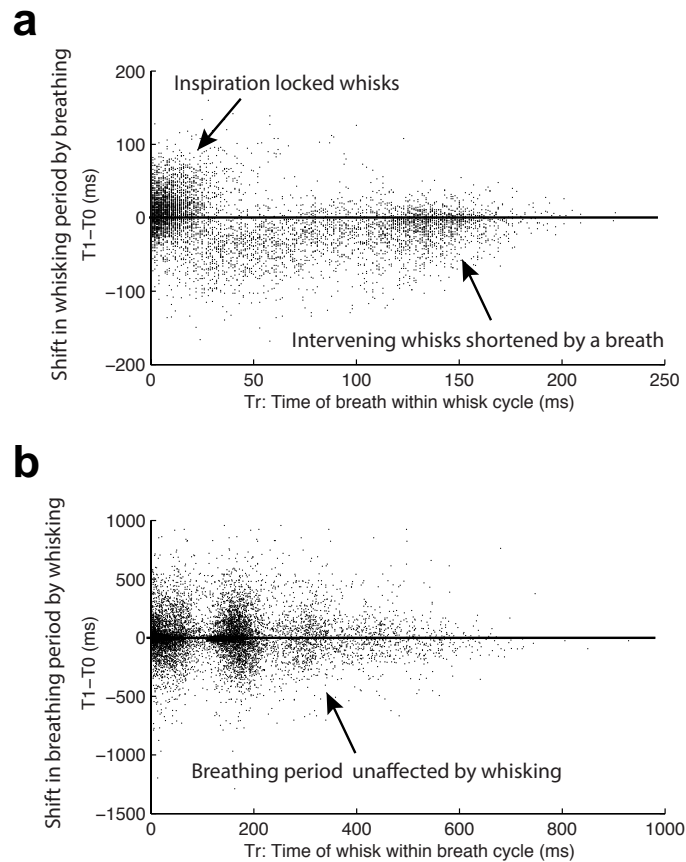


Figure S5. Response of the whisking rhythm to breathing versus the breathing rhythm to whisking

To emphasize the asymmetric interaction between whisking and breathing, we plot the shift in period ($T_1 - T_0$) of each behavior as a function of the time within the cycle when the other behavior occurs (treset). As in **Figure S4**, T_0 represents the expected period of the perturbed behavior, taken as the period of the cycle prior to that which contains an interrupting event, and T_1 represents the interrupted period. Unlike **Figure S4**, both sniffing and basal respiratory frequencies are included in the analysis to permit a symmetric comparison between the response of whisking to breathing and the response of breathing to whisking.

(a) Shift in whisking period ($T_1 - T_0$) relative to the reset by an inspiration (at times treset). As in **Figure S4**, there is a bias for the intervening whisks to be shortened by the onset of breathing during basal respiration. The inhalation locked whisks during sniffing are not in steady state and not so constrained.

(b) Shift in respiratory period ($T_1 - T_0$) relative to the reset by a vibrissa protraction (at times treset). There is no apparent bias for the period of breathing to be shifted by the presence of a whisk during either sniffing or basal respiration.

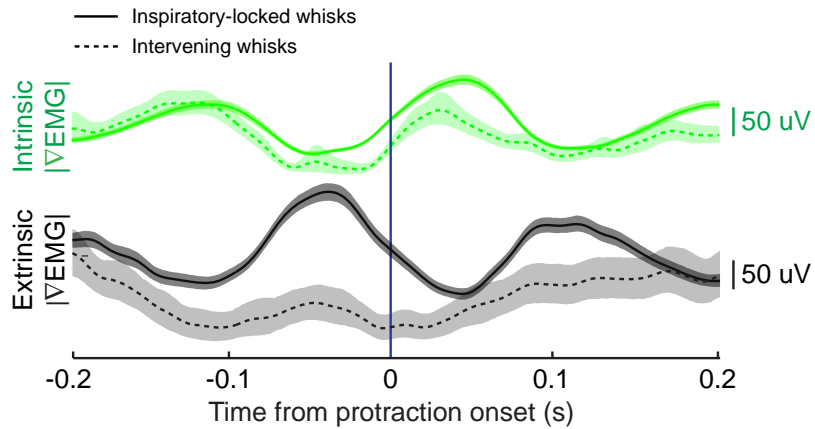


Figure S6. Cross-correlation between EMG activity and vibrissa movement.

Cross-correlation of the smoothed $|\nabla\text{EMG}|$ for intrinsic (green) and extrinsic (black) muscles with the protraction onset times for inspiratory and intervening whisks. Solid traces represent correlation with inspiratory whisks and dashed traces represent correlation with intervening whisks. Bands represent 95 % confidence intervals.

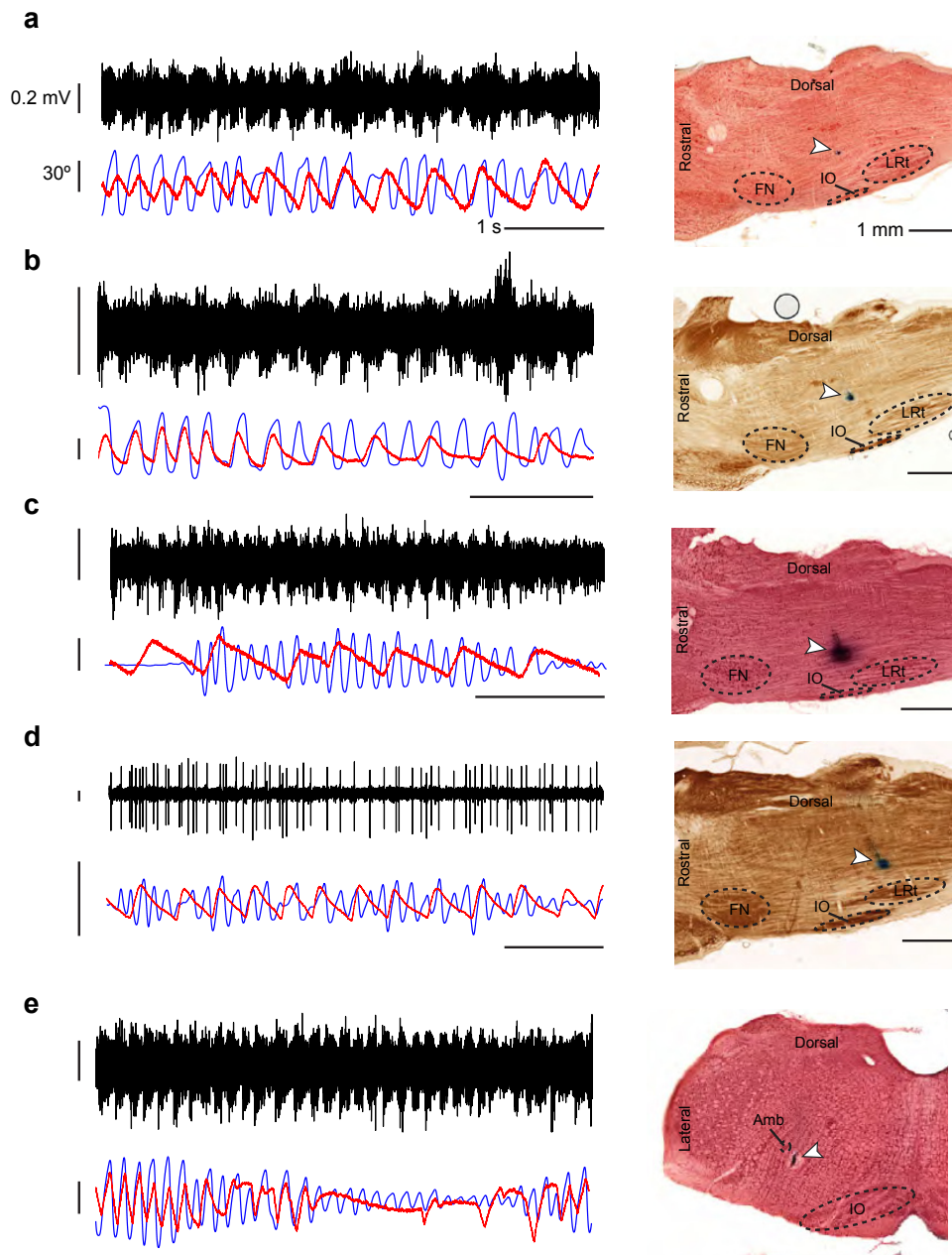


Figure S7. Compendium of spiking records from all vIRt whisking units during breathing and whisking in alert rats.

(a-e) Concurrent recordings of breathing (red), whisking (blue), and multiunit spike activity (black) in the IRt for all whisking units. The location of the recording site labeled with Chicago sky blue is shown on the right a sagittal section (panels a to d) or coronal section (panel e) counterstained with neutral red (panels a, c, and e) or cytochrome oxidase (panels b and d). Landmarks, including the facial nucleus (FN), inferior olive (IO), lateral reticular nucleus (LRt), and ambiguous nucleus (Amb), are outlined in black. Arrowheads mark the labeled recording site. Scale bars are as defined in panel a.

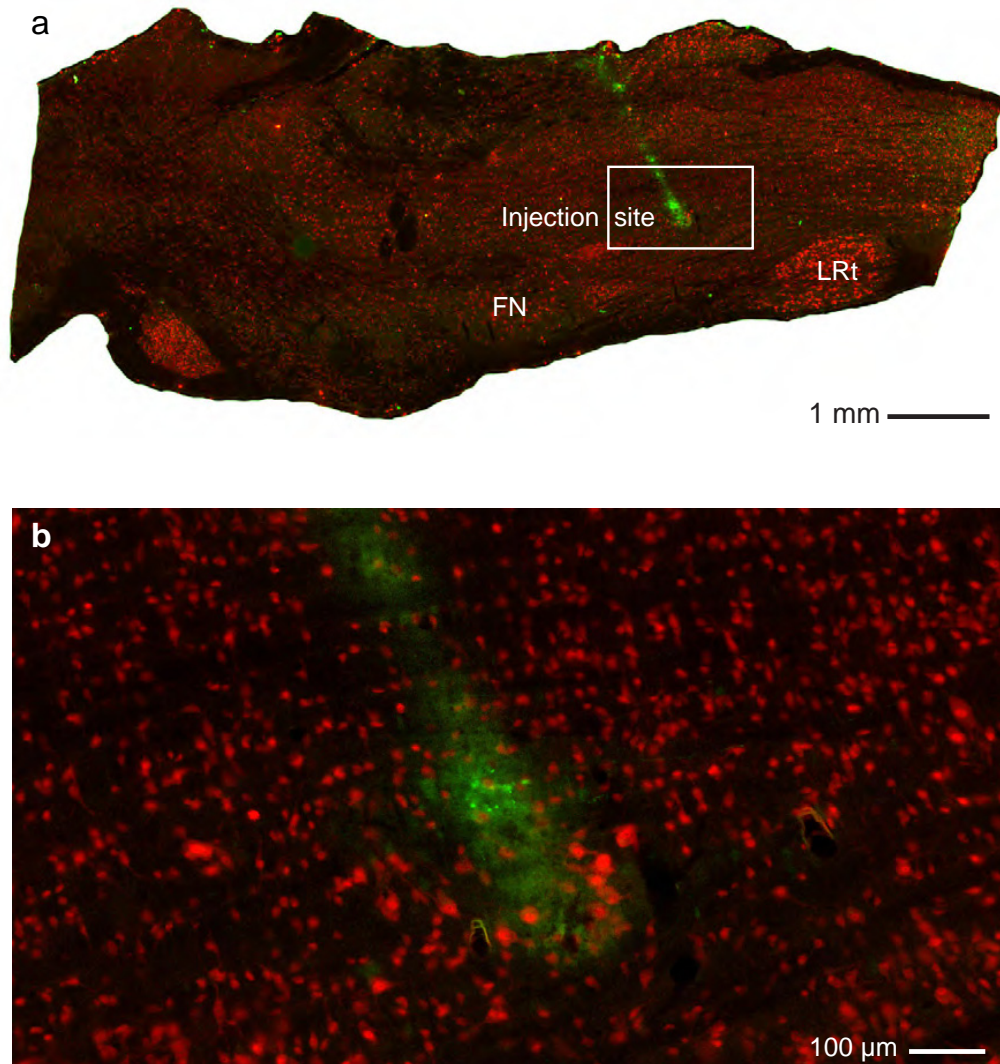


Figure S8. Kainic acid injection site and surrounding brainstem tissue.

Injection at this site resulted in sustained, coordinated ipsilateral whisking. Whisking appeared normal the day following the injection and thereafter (data not shown).

(a) The injection site is labeled with biotinylated dextran amine, and the tissue is counterstained with an antibody against neuronal nuclear protein after three days of recovery.

(b) Magnified view of the white box in panel a. Cells around the injection site remain intact.

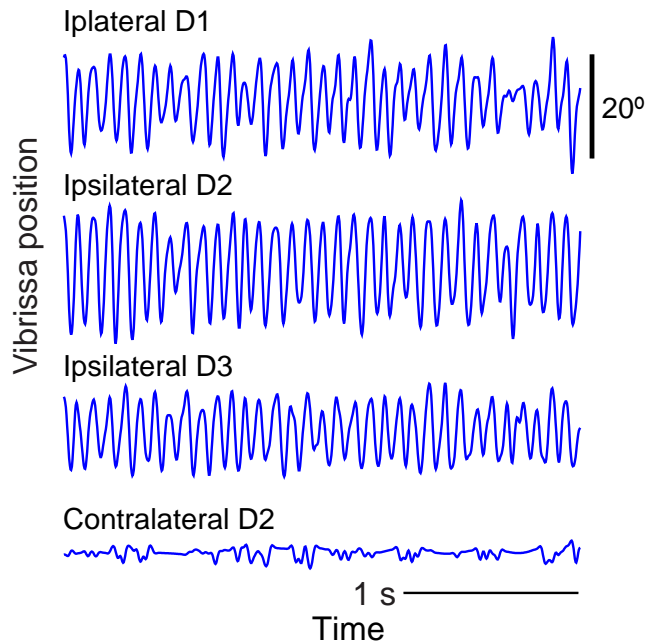


Figure S9. Coordinated movement of ipsilateral vibrissae following kainic acid injection in the vicinity of the vIRT

Simultaneously recorded motion of three neighboring vibrissae, *i.e.*, D1, D2 and D3, on the ipsilateral side, and the D2 vibrissa on the contralateral side, after activation of whisking by kainic acid injection.

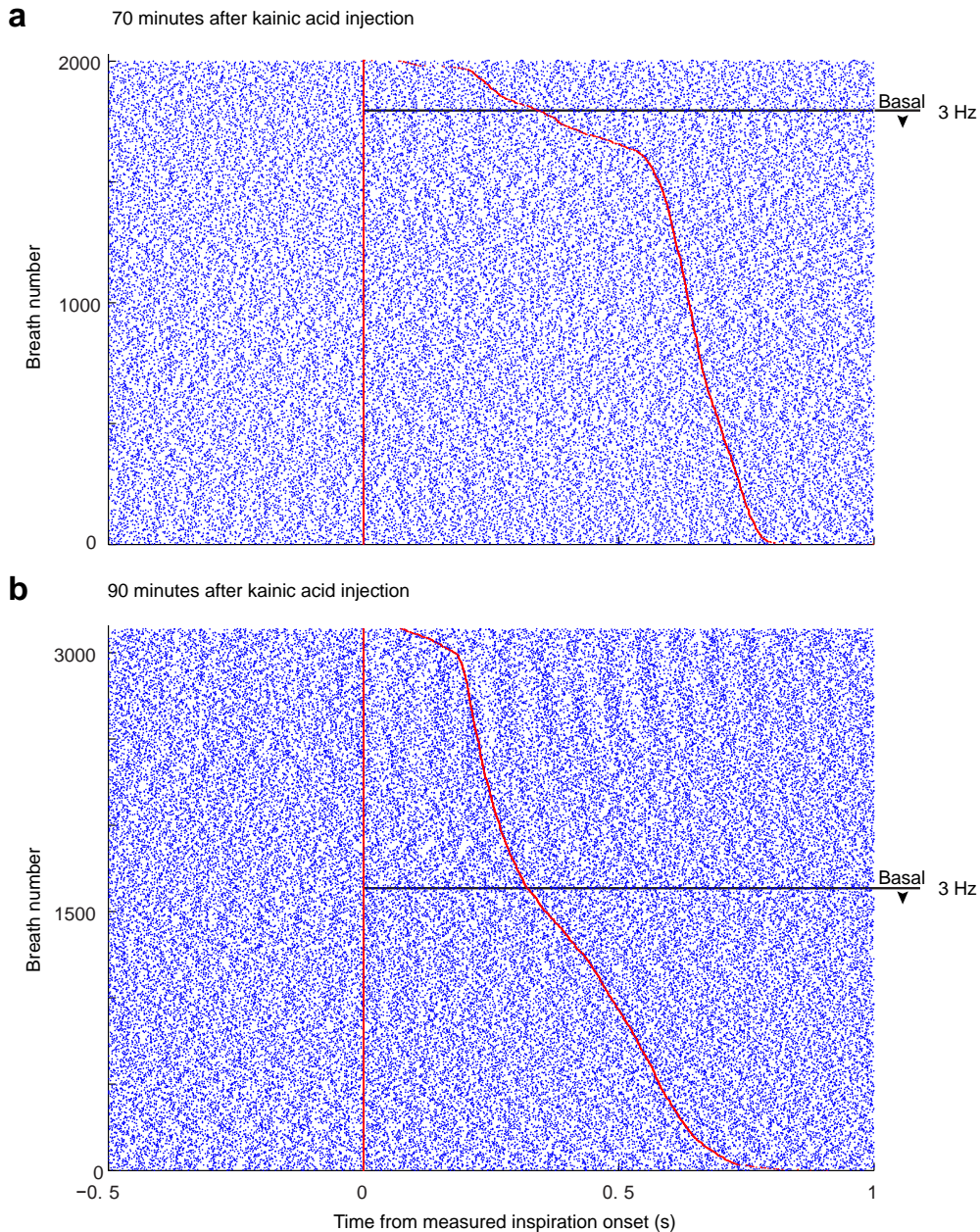


Figure S10. Lack of coordination of kainic acid-induced whisking and breathing.

Temporal relationship between whisking and breathing events for kainic acid induced whisking in the lightly anesthetized rat. Raster plots of inspiration (red dots) and protraction (blue dots) onset times relative to each breath are sorted by the duration of the breath.

(a) At basal respiratory frequencies, correlation with event times was low and significant in only one of eleven different twenty minute epochs ($p < 0.01$) across three animals; shown here is this single case.

(b) The correlation of the remaining ten out of the eleven epochs was found to be statistically insignificant ($p > 0.05$); one of the ten cases is shown here.

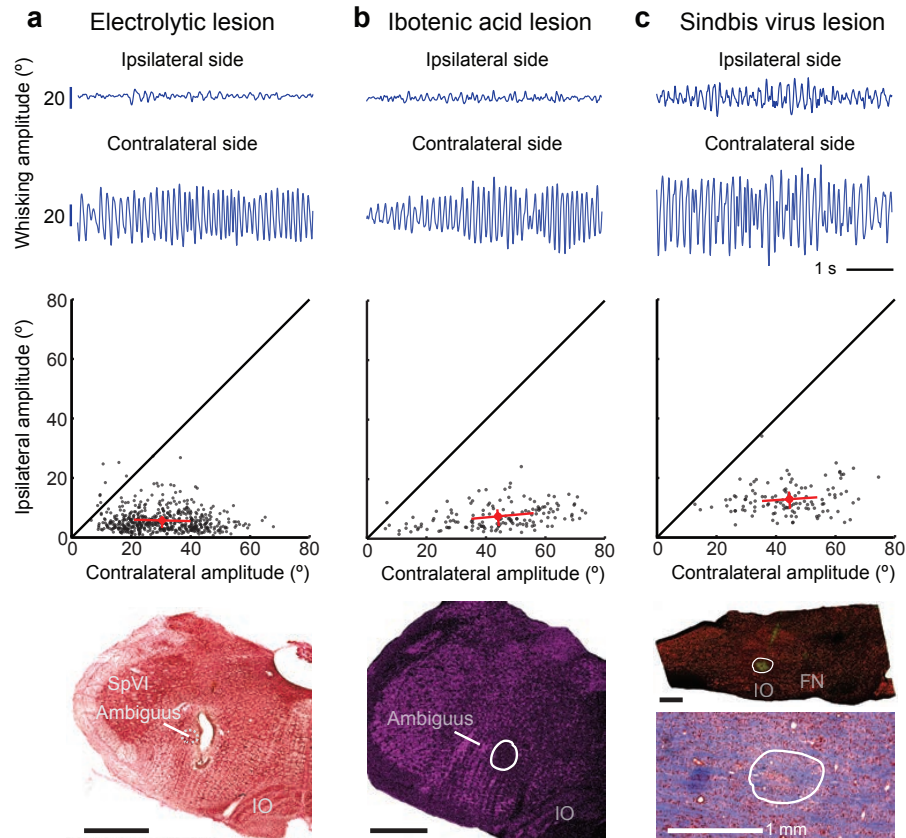


Figure S11. Three different methods of lesion in the vIRt that result in ipsilateral whisking impairment

(a) Example of whisking bout following an electrolytic lesion in the vIRt (top). As in **Figure 5**, a full analysis of ipsilateral versus contralateral whisk amplitudes reveals the functional completeness of the lesion (middle; each dot represents one whisk, circle represents the mean, and lines represent the inter-quartile range). Histological analysis confirms that the lesion is in the vIRt; coronal section stained with neutral red (bottom). This panel is a replication of **Figure 5a**, included here for comparison to other lesion methods.

(b) Example of a whisking bout after an excitotoxic lesion in the vIRt made by pressure injection of ibotenic acid (top). The analysis of whisking amplitudes (middle) is as in panel a. The histological section (bottom) shows the extent of neuronal degeneration after staining with α -NeuN.

(c) Example of a whisking bout after a lesion in the vIRt made by microinjection of a Sindbis viral vector that codes for the expression of green-fluorescent protein (top). The analysis of whisking amplitudes (middle) is as in panels a and b, and the histology (bottom) is as in panel b. We further show an adjacent 30 μ m section stained with Luxol fast blue to label myelin and neutral red to label Nissl bodies; the outlined region corresponds to the location where there was a loss of cells as revealed by the α -NeuN staining.

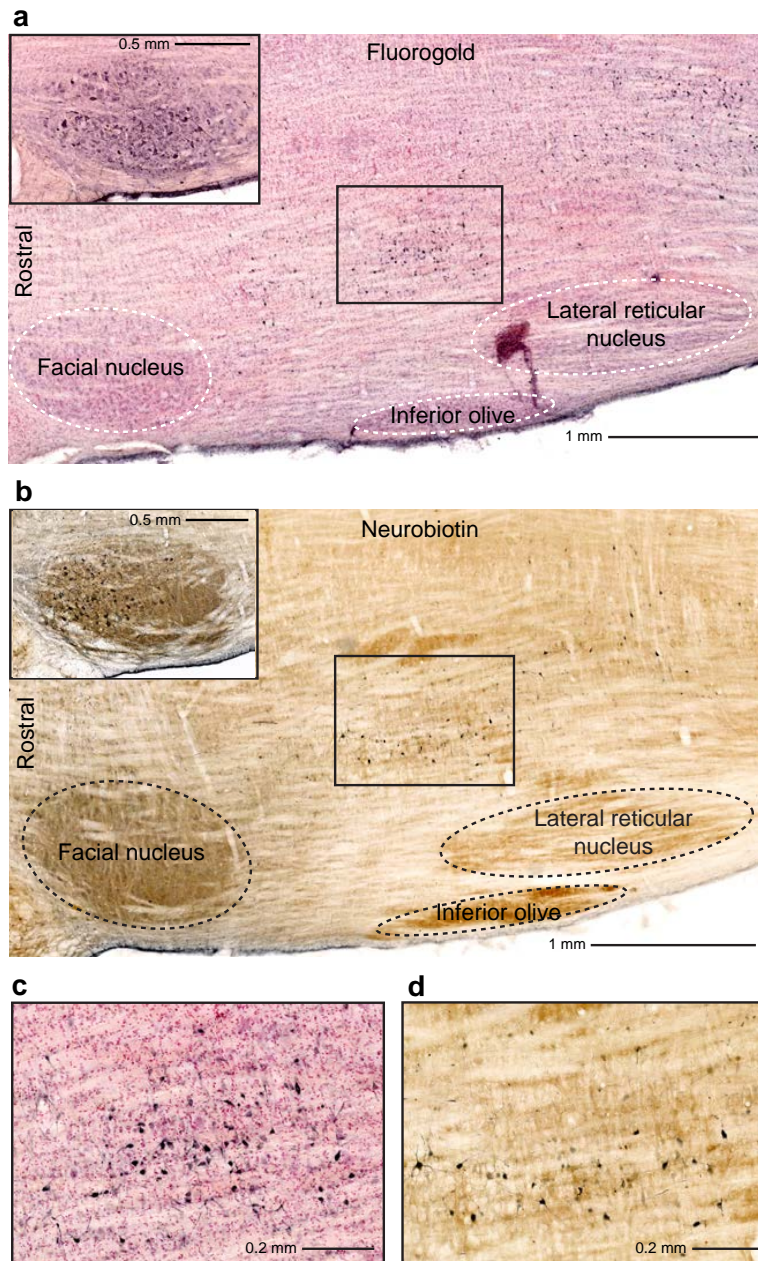


Figure S12. Fluoro-Gold™ and Neurobiotin™ retrogradely label vIRt cells that project to the facial motor nucleus.

(a) Cells are retrogradely labeled in vIRt and PCRt following an injection of Fluoro-Gold™ in the lateral aspect of the facial nucleus (inset). Sagittal section.

(b) A similar pattern of labeling is observed after injection of Neurobiotin™ into the lateral facial nucleus (inset).

(c-d) Magnification of the vIRt regions outlined in panels a and b, respectively.

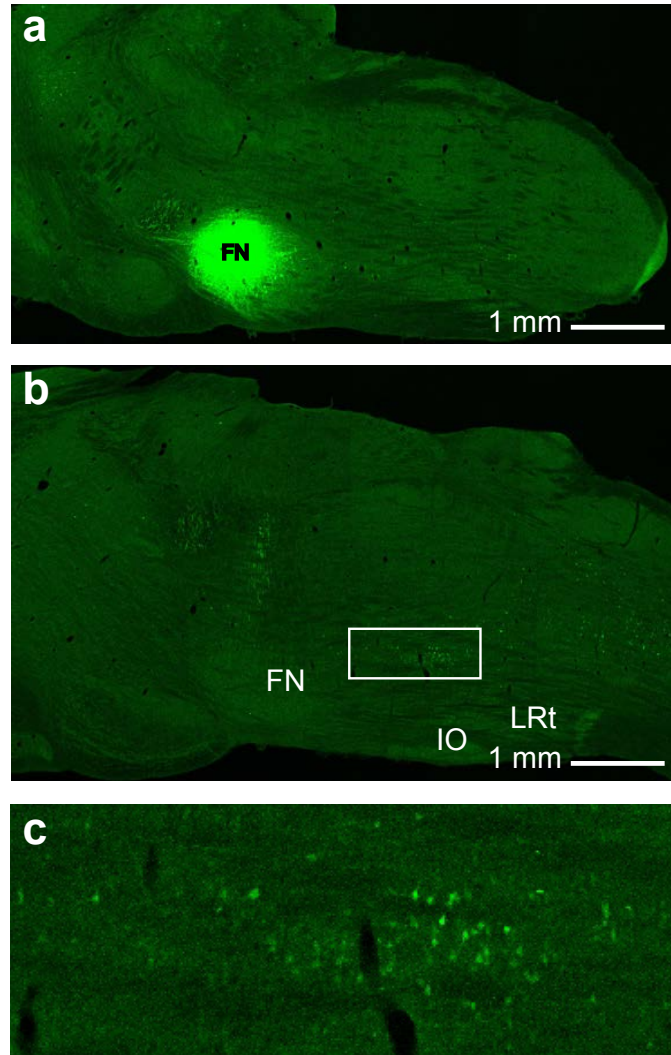


Figure S13. Fluoro-Gold™ retrograde labeling for characterization of the neurotransmitter phenotypes of facial pre-motoneurons.

(a) Example of a Fluoro-Gold™ injection site in the lateral facial nucleus.

(b) Region in which counts of cells double-labeled with Fluoro-Gold™ and in situ hybridization for vGluT2, GlyT2, or GAD67 were performed.

(c) Magnified view of the cell counting region in panel **b**.

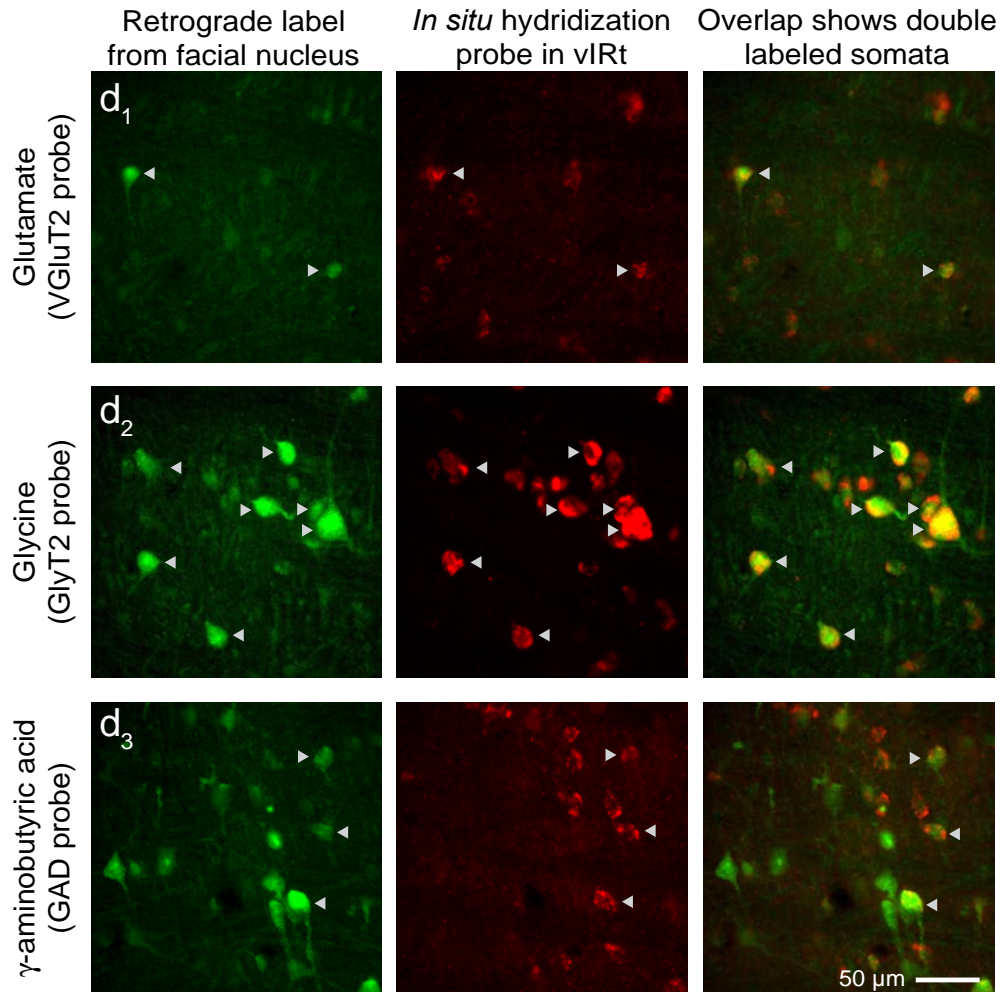


Figure S14. Determination of the neurotransmitter phenotype of neurons that project from the vIRt to the facial motoneurons that drive protraction of the vibrissae.

Neurons were labeled via retrograde transport of Fluor-Gold™ from the lateral aspect of the facial nucleus (left column) and the tissue was processed for *in situ* hybridization (middle column) with probes for glutamate (top row), glycine (middle) and γ -aminobutyric acid (bottom). The merged images (right column) reveal double-labeled cells, denoted with arrows.